Dalton Transactions

ROYAL SOCIETY OF CHEMISTRY

PAPER

View Article Online
View Journal | View Issue

Cite this: *Dalton Trans.*, 2026, **55**, 3723

Stratified sulfatometallates: unlocking a new dimension in sulfatomolybdates

Vivien Wessels,[a] Jasper Arne Baldauf,[b] Rainer Pöttgen [b] and Henning A. Höppe *[a]

Received 22nd December 2025,
Accepted 22nd January 2026

DOI: 10.1039/d5dt03061g

rsc.li/dalton

Thus far, only a few sulfatomolybdates are known. Their anions feature mainly low dimensionalities. By choosing appropriate reaction conditions, new compounds, namely, β-$K_2[MoO_2(SO_4)_2]$ and $Na_2[MoO_2(SO_4)_2]$, are synthesised, which revealed layered structures for the first time for this class of materials. These compounds comprise sulfate tetrahedra and molybdate octahedra connected *via* common edges, forming a *vierer ring* between the building units. While the potassium cations are fully ordered in β-$K_2[MoO_2(SO_4)_2]$, the sodium cations exhibit disorder in $Na_2[MoO_2(SO_4)_2]$, which does not order at higher temperatures. Additionally, the compound crystallises in an incommensurate modulated structure at room temperature, which orders at higher temperatures. The titled compounds were characterised by single-crystal and powder XRD, MAPLE calculations, FT-IR spectroscopy, UV-vis spectroscopy, magnetic susceptibility analysis and thermogravimetric analysis (TGA). The latter reveals fairly high thermal stabilities for both compounds.

Introduction

In solid-state chemistry, layered structures offer various opportunities for the development of advanced materials with diverse functionalities. They offer the advantages of high energy densities and stabilities, which make them suitable for applications in batteries and energy storage materials.[1–4] Additionally, the optical properties might be enhanced in structures with higher anion dimensions. With increasing anion dimensionality, the stiffness of the whole structure increases, thereby reducing the vibrational loss of luminescence intensity. Luminescence properties are also enhanced by the absence of a local inversion centre, allowing mixing of orbitals on the basis of the parity selection rule. The probability of the absence of local inverstion centres is enhanced in silicate-analogous materials due to their tetrahedral buildung units. Thus, silicate-analogous materials have a higher chance of forming non-centrosymmetric structures because their tetrahedral building units do not feature inversion symmetry.[5–9] Sulfatomolybdates–a rather young and thus unexplored material class–can be considered silicate-analogous materials; for example, tetrahedral sulfate and molybdates are reasonable building units. Molybdates are also capable of forming octahedra as observed in the known sulfatomolybdates such as $Rb_2[Mo_3O_6(SO_4)]$,[10] α-$K_2[MoO_2(SO_4)_2]$,[11] γ-$K_2[MoO_2(SO_4)_2]$,[12] $A_4[MoO_2(SO_4)_3]$ (where A = Na or K),[13,14] and $K_8[(MoO_2)_2(SO_4)_6]$. Fig. 1 emphasises how much underexplored is the field of sulfatomolybdates. Only six different structure types are known, mostly comprising low-dimensional anionic substructures. Recently, we reported the first sulfatomolybdate with a three-dimensionally condensed anion, *i.e.* α-$K_2[MoO_2(SO_4)_2]$.[11] This is an astonishing finding since one would expect a high repulsion between the formally highly charged S^{6+} and Mo^{6+} polyhedral centres.

Hence, we present the very first 2D sulfatomolybdate substructure in this study. A closer look at the periodic table makes the novelty of this material class even more obvious because only alkali metal compounds have been known to date (Fig. 1). Further investigation by exploring other metal cations might be promising. For instance, introducing rare-earth elements could enhance the luminescence properties as molybdates may act as antenna.[15,16] Molybdates can be excited *via* an allowed ligand to metal charge transfer (LMCT); to enhance the parity forbidden f–f transitions of the rare-earth ions by an energy transfer. Thus, quantum efficiencies of 100% are possible. A further advantage is the high thermal stability of these compounds, as shown by recent studies.[11] This makes them suitable for applications such as LED materials in the future.

Herein, we synthesise two new compounds β-$K_2[MoO_2(SO_4)_2]$ and $Na_2[MoO_2(SO_4)_2]$ and characterize them by single-crystal and powder X-ray diffraction, magnetic measurements, FT-IR spectroscopy, UV-vis spectroscopy, and thermogravimetric analysis (TGA). We synthesised both these compounds in their

[a]*Professur für Festkörperchemie und Materialwissenschaften, Institute of Physics, Universität Augsburg, Universitätsstraße 1, 86159 Augsburg, Germany. E-mail: henning.hoeppe@physik.uni-augsburg.de*
[b]*Institut für Anorganische und Analytische Chemie, Universität Münster, Corrensstraße 30, 48149 Münster, Germany*

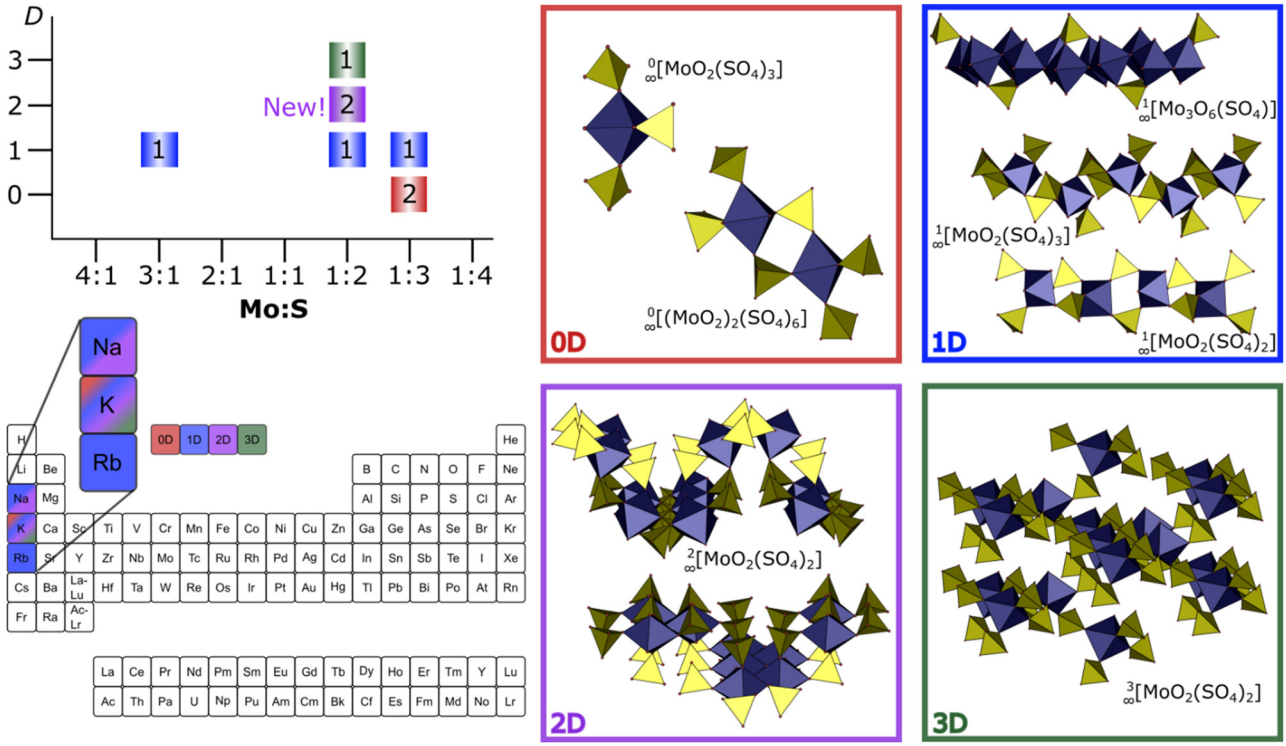

Fig. 1 Overview of known sulfatomolybdates: the graph in the upper left shows the number and dimension *D* of known sulfatomolybdate substructures with respect to their molar ratio between molybdenum and sulfur. 2D compounds are reported for the first time in this work. The periodic table in the lower left emphasises how underexplored this material class is, only compounds featuring alkali metal cations are discovered yet. The coloured boxes on the right show the structural motifs of sulfatomolybdates ordered by their anion dimensionality.

phase-pure form by controlling the synthesis conditions carefully. Eventually, we compared them with their respective polymorphs.

Results and discussion

Crystal structure

β-$K_2[MoO_2(SO_4)_2]$ marks the new third phase of this composition and crystallises in the monoclinic space group $P2_1/c$ (no. 14) with four formula units per unit cell (Fig. 2). While γ-$K_2[MoO_2(SO_4)_2]$[12] exhibits a 1D and α-$K_2[MoO_2(SO_4)_2]$[11] a 3D anionic substructure, β-$K_2[MoO_2(SO_4)_2]$ shows a new connection of the fundamental building unit by forming corrugated layers. The compounds are classified after their densities (α-$K_2[MoO_2(SO_4)_2]$: 2.917 g cm^{-3}, β-$K_2[MoO_2(SO_4)_2]$: 2.888 g cm^{-3}, γ-$K_2[MoO_2(SO_4)_2]$: 2.863 g cm^{-3}), which correlate with their dimensionalities. So far, there seems to be no synthetic way to transform the phases into each other. In β-$K_2[MoO_2(SO_4)_2]$, all atoms are situated on the general Wyckoff position 4*e*. The fundamental building unit (FBU) consists of a molybdate octahedron and two sulfate tetrahedra connected by common corners. The polyhedron deviations calculated by the method of Balić-Žunić and Makovicky[17,18] remain small for the sulfate tetrahedra (S1: −0.08% and S2: −0.09%); these can therefore be classified as regular. In contrast, the molybdate octahedron shows a larger deviation of −1.65% caused by the high repulsion of the neighbouring highly charged sulfate centres. This leads to shorter bonds of molybdenum towards the terminal oxygen atoms (Mo–O1: 167 pm and Mo–O2: 168 pm). The expected bond length calculated after Shannon's radii[19] is 195 pm, which is close to the averaged value of the crystal structure data with 197 pm. Selected bond lengths and angles are listed in

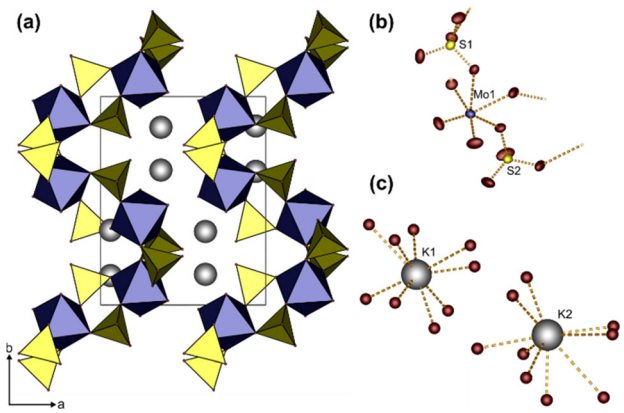

Fig. 2 Unit cell of β-$K_2[MoO_2(SO_4)_2]$ (a), fundamental building unit (b) and coordination environment of the potassium cations (c); sulfate tetrahedra: yellow, molybdate octahedra: violet, potassium cations: grey, and oxygen: red. Ellipsoids are set to a probability of 50%.

Table 1 Selected interatomic distances (pm) and angles (°) of β-$K_2[MoO_2(SO_4)_2]$ and $Na_2[MoO_2(SO_4)_2]$. Standard deviations are given in parentheses

	β-$K_2[MoO_2(SO_4)_2]$	$Na_2[MoO_2(SO_4)_2]$
A–O (A = Na or K)	266.6(2)–337.0(3)	
$\sum r_{ion}$ (A–O)	291	
Mo–O^{term}	167.5(2)–168.4(2)	168.0(3)–168.2(3)
Mo–O^{br}	198.1(2)–225.94(19)	201.8(2)–218.7(3)
S–O^{term}	142.65(28)–144.14(24)	142.1(4)–143.6(4)
S–O^{br}	146.7(2)–152.9(2)	146.2(4)–152.2(3)
O–Mo–O	75.81(8)–166.03(11)	76.03(12)–166.87(16)
O–S–O	104.00(12)–114.09(15)	105.6(2)–114.7(2)
Mo–O–S1	128.08(12)–140.79(13)	130.71(19)–142.7(2)
Mo–O–S2	134.43(13)–143.16(13)	128.6(2)–135.2(2)

Table 1. The average S–O bonds of 148 pm for $[SiO_4]^{2-}$ and 147 pm are close to the expected value of 148 pm, whereas the bonds of the bridging oxygen atoms towards the molybdenum centres are slightly lengthened due to repulsion. The corresponding ionic radii are listed in Table S8. Both the potassium cations are coordinated by nine oxygen atoms, as proven by MAPLE calculations.[20–23] The average K–O bond lengths (K1–O: 289 pm and K2–O: 304 pm) lie around the value of 291 pm calculated by considering a nine-fold coordination for potassium.[19]

It is striking that the anion dimensionality depends on the connection of the polyhedra, comparing the structural motifs of the anionic network structures of α-, β- and γ-$K_2[MoO_2(SO_4)_2]$.[11,12] In the 1D γ-$K_2[MoO_2(SO_4)_2]$, the sulfate tetrahedra and molybdate octahedra are connected continuously *via vierer rings* (Fig. 3, red connections) yielding infinite chains, while the connection opens in the 2D β-$K_2[MoO_2(SO_4)_2]$ towards different molybdenum atoms, so that only one *vierer ring* remains and a layered anion is achieved. In α-$K_2[MoO_2(SO_4)_2]$, no *vierer ring* is left and a 3D network is formed. Thus, the dimensional loss comes with building *vierer rings* in the anion.

At room temperature, $Na_2[MoO_2(SO_4)_2]$ crystallises in the monoclinic superspace group $P2_1/n(\alpha 0\gamma)00$ (no. 14) with a single modulation vector q = (0.546(3), 0, 0.286(4)) and four formula units per unit cell as an incommensurately modulated structure with an additional disorder of the sodium cations (Fig. 4). The reciprocal space shows satellite reflections (Fig. S1) which order with increasing the temperature beyond 50 °C. Then, the structure orders and crystallises in the orthorhombic space group *Pbcn* (no. 60) with eight formula units per unit cell, whereas the disorder of the sodium cations remains. Decreasing the temperature did not lead to a reduction of the satellites. In the monoclinic case, all atoms are assigned to the general Wyckoff position 4*e* except for Na10, which is assigned to the special position 2*c*. The anion forms layers in the *a*–*c* plane (Fig. 4a). The FBU consists of one molybdate octahedron and two sulfate tetrahedra connected *via* common corners. The polyhedron deviation in $Na_2[MoO_2(SO_4)_2]$ is similar to that of the potassium compound

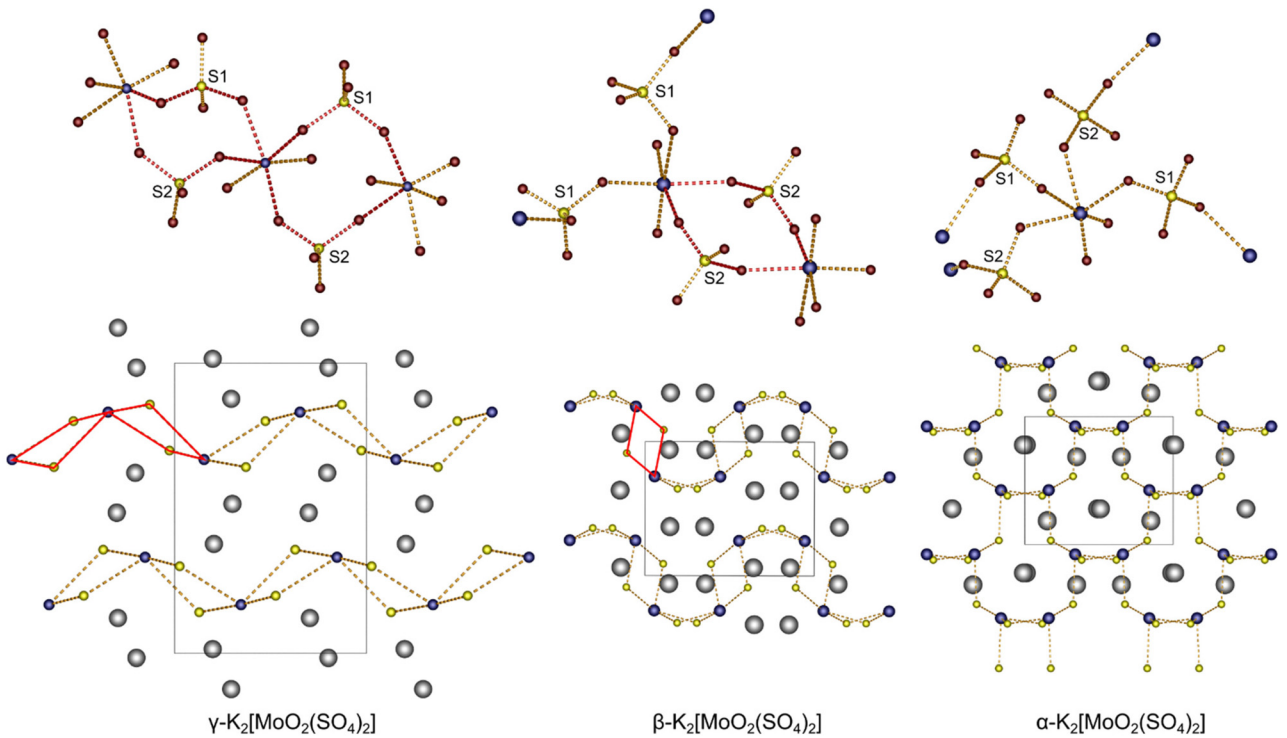

Fig. 3 Relationship between the number of *vierer rings* (red bonds) in the polymorphs of $K_2[MoO_2(SO_4)_2]$ and anion dimensionality. The number of *vierer rings* decreases with higher dimensions. For better understanding, oxygen atoms are omitted in the unit cells and only connections between sulfate and molybdate centres are shown; sulfur: yellow, molybdenum: violet, potassium: grey, and oxygen: red.

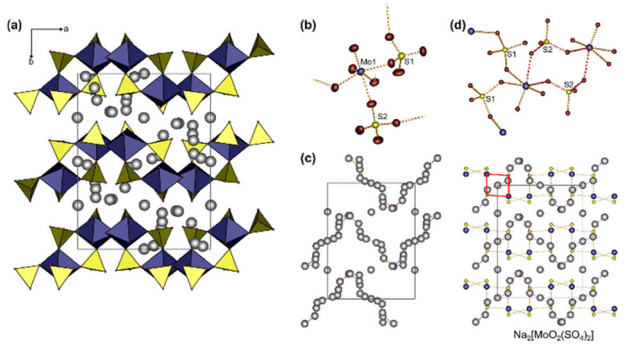

Fig. 4 Unit cell of $Na_2[MoO_2(SO_4)_2]$ (a), fundamental building unit (b), sodium disorder (c) and number of *vierer rings* (red bonds) (d); sulfate tetrahedra: yellow, molybdate octahedra: violet, sodium cations: grey, and oxygen atoms: red. Ellipsoids in (b) are set to a probability of 50%. In (d), the high temperature phase is shown for a better comparison with potassium compounds. Also, the number of sodium cations was reduced in (d) for a better view on the sulfur and molybdenum centres.

for the sulfate tetrahedra (S1: −0.18% and S2: −0.07%).[17,18] The molybdate octahedron shows a clearly larger deviation of −8.60% with a considerable centroid shift of 35 pm. Considering the molybdenum "centre" in the octahedron, the molybdenum is shifted away from the plane connected to the three sulfate tetrahedra due to the repulsion between the Mo^{6+} and S^{6+} centres (Fig. S3). Nevertheless, the average Mo–O and S–O bond lengths are in good accordance with the sum of the ionic radii according to Shannon.[19] The average Mo–O bond length is 196 pm (Shannon: 196 pm); the average bond lengths in the sulfate groups range between 147 pm in $[S1O_4]^{2-}$ and $[S2O_4]^{2-}$ to 146 pm in $[S3O_4]^{2-}$ and $[S4O_4]^{2-}$ (Shannon: 148 pm). The coordination number of the sodium atom strongly depends on the disorder. We chose the sodium cations with the highest fractional occupation factors, *i.e.*, Na1, Na2 and Na3 (Table S2), as representatives for the discussion of the bond lengths with respect to their coordination number (Fig. S5). According to MAPLE calculations,[20–23] Na1 is coordinated by eight oxygen atoms, while Na2 and Na3 are coordinated sevenfold. The average bond lengths are 263 pm (Na1–O), 253 pm (Na2–O) and 250 pm (Na3–O). This fits quite well with the sum of the ionic radii after Shannon[19] between 265 pm (CN = 8) and 250 pm (CN = 7).

The structural motifs of $Na_2[MoO_2(SO_4)_2]$ are similar to those of β-$K_2[MoO_2(SO_4)_2]$. The formation of *vierer rings* in the anion leads to the layered structure, which seems to be flattened in $Na_2[MoO_2(SO_4)_2]$ compared to the potassium compound. This is also reflected in the Mo–O–S2 angles, where $Na_2[MoO_2(SO_4)_2]$ tends to have smaller angles inside the *vierer ring* (Table 1). This is indicated by the red squares in Fig. 3 and 4d.

The modulation affects the sodium cations in particular. While the molybdate and sulfate units show nearly no or only small modulation, the sodium cations show large sinoidal positional and occupational amplitudes along the modulation axis t. This is clearly seen in the de Wolff section (Fig. S2). The occupation factors vary along the modulation axis as well; certainly, the modulated occupation factor of a sodium site becomes small if another sodium site with high occupation comes close. The disordered sodium ions are arranged along chains. Surprisingly, these chains are not situated clearly between the layers in the *ac*-plane but meander through the anion layers (Fig. 4c and d).

A reasonable explanation for the modulation is incommensurate repulsion between the sodium ions, as well as incommensurate attraction to the coordinating oxygen atoms. Below the lock-in temperature, neither conflicting interaction can find a commensurate vibrational solution. Moreover, the reduced sodium content of the compound presumably is established at the elevated synthesis temperature; at room temperature, the local charge disbalances, where selected Mo^{5+} are doped instead of Mo^{6+}, might cause this modulation.

Synthetic approach

Both β-$K_2[MoO_2(SO_4)_2]$ and $Na_2[MoO_2(SO_4)_2]$ were synthesised phase-pure, as depicted in the powder X-ray diffraction (PXRD) patterns in Fig. 5. Interestingly, the synthesis of β-$K_2[MoO_2(SO_4)_2]$

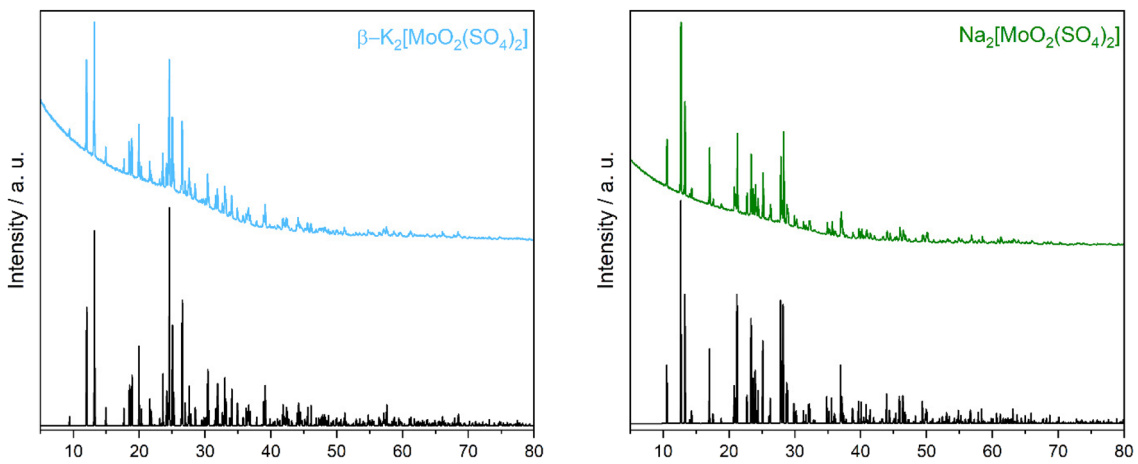

Fig. 5 Experimental X-ray diffraction patterns compared with the theoretical XRD patterns for β-$K_2[MoO_2(SO_4)_2]$ and $Na_2[MoO_2(SO_4)_2]$.

differs only in one aspect from that of α-$K_2[MoO_2(SO_4)_2]$.[11] In both cases, MoO_3 and $K_2S_2O_7$ are ground and transferred into a silica ampoule which is then sealed under vacuum. The first step of the furnace program at 420 °C was necessary to melt $K_2S_2O_7$ and the second one to crystallise the desired products. The syntheses follow the simple reaction equation:

$$A_2S_2O_7 + MoO_3 \rightarrow A_2[MoO_2(SO_4)_2], \quad (1)$$

where A = Na or K. Between the two heating steps, it is crucial to grind the intermediate products. When grinding in air, the 3D α-$K_2[MoO_2(SO_4)_2]$ forms, while grinding in an argon filled glovebox before loading the silica ampoule again yields 2D β-$K_2[MoO_2(SO_4)_2]$. Both syntheses are reproducible and lead to phase pure products. Since it is not possible to achieve a perfect vacuum condition, the remaining traces of air or argon in the ampoule might be the decisive reason for the formation of different compounds; remaining moisture as reaction agents was improbable, since the ampoule was heated to 180 °C before filling. This might also lead to different colour impressions, as β-$K_2[MoO_2(SO_4)_2]$ exhibits a light blue and α-$K_2[MoO_2(SO_4)_2]$ a dark blue colour.[11] It is known that the origin of coloured oxides can depend on the annealing atmosphere, *e.g.* the remaining gas in the ampoule.[24,25] It may cause oxygen vacancies, which in turn affect the oxidation state of molybdenum in the material. The colour impressions of the titled compounds are further discussed in the UV-vis part. Both structures, α-$K_2[MoO_2(SO_4)_2]$ and β-$K_2[MoO_2(SO_4)_2]$, are not convertible into each other when grinding the product under the opposite environments, air or argon, and heating again at 280 °C in a sealed ampoule. We could not reproduce the third phase γ-$K_2[MoO_2(SO_4)_2]$. In contrast to the potassium compound, $Na_2[MoO_2(SO_4)_2]$ forms independent of grinding in air or under argon and using vacuum or not in the sealed ampoule.

Our recent work includes the sulfatomolybdates $Na_4[MoO_2(SO_4)_3]$ and $K_8[(MoO_2)_2(SO_4)_6]$. The synthesis conditions underline the complexity of these reactions, since, apart from one additional starting material, *i.e.*, A_2SO_4 (A = Na or K), the synthesis conditions were the same as in this contribution. Nevertheless, all syntheses lead to phase pure products.

Electrostatic calculations

Electrostatic consistency was proven by the calculations based on the Madelung part of lattice energy (MAPLE) concept.[20–23] The single-crystal data of β-$K_2[MoO_2(SO_4)_2]$ and $Na_2[MoO_2(SO_4)_2]$ were compared with the summation of the respective binary and ternary compounds (Table 3 and S10). The deviations remain at 0.52% and 0.14%, below the mark of 1%, which indicates the electrostatic consistency of the structural models. We point out that the sodium atoms in $Na_2[MoO_2(SO_4)_2]$ are slightly over-occupied according to the structural refinement with Jana2020.[26] We compared the values of the binary compounds stoichiometrically to the assumed composition $Na_2[MoO_2(SO_4)_2]$, neglecting the under-

Table 2 Crystal data and the details of the structural refinements of β-$K_2[MoO_2(SO_4)_2]$ and $Na_2[MoO_2(SO_4)_2]$ determined by single-crystal X-ray diffraction. Standard deviations are given in parentheses

	β-$K_2[MoO_2(SO_4)_2]$	$Na_2[MoO_2(SO_4)_2]$	$Na_2[MoO_2(SO_4)_2]$
Temperature (K)	298(2)	293(2)	373(2)
Molar weight (g mol^{-1})	398.26	366.04	366.04
Crystal system	Monoclinic	Monoclinic	Orthorhombic
Space group	$P2_1/c$ (no. 14)	$P2_1/n(\alpha 0\gamma)00$ (no. 14) q = (0.546(3), 0, 0.286(4))	$Pbcn$ (no. 60)
a (Å)	9.5122(4)	12.6106(2)	12.6264(7)
b (Å)	11.8520(4)	16.6905(3)	7.8092(5)
c (Å)	8.2378(3)	7.8176(4)	16.7150(11)
β (°)	99.470(2)	90.0760(10)	90
V (Å^3)	916.06(6)	1645.43(9)	1648.13(18)
Z	4	4	8
ρ (g cm^{-3})	2.89	2.96	2.95
Absorption coefficient μ (mm^{-1})	2.8	2.2	2.2
F(000)/e	768	1409	1408
Radiation; wavelength λ (Å)	0.71073	0.71073	0.71073
Diffractometer	Bruker D8 venture	Bruker D8 venture	Bruker D8 venture
θ range (°)	2.171–32.482	2.34–31.66	2.437–28.015
Absorption correction	Multi-scan	Multi-scan	Multi-scan
Transmission (min; max)	0.687; 0.748	0.609; 0.7234	0.654; 0.746
Index range $h/k/l/m$	±14/±17/±12	±19/±24/±11/±1	±16/±10/±22
Reflections collected	61 922	65 377	84 892
Obs. reflections	3310	15 465	2002
Refined parameters	136	649	162
R_{int}	0.0725	0.0804	0.1262
R_1 (all data)	0.0387	0.1335	0.0473
wR_2	0683	0.1690	0.0992
GooF	1.104	1.8436	1.125
Residual electron density (max; min) (e$^-$)	0.66; −0.72	1.01; −1.28	0.97; −0.72
CSD	2518135	2518136	2518137

Table 3 Calculated MAPLE values of β-$K_2[MoO_2(SO_4)_2]$ and $Na_2[MoO_2(SO_4)_2]$ compared with that of the binary compounds

β-$K_2[MoO_2(SO_4)_2]$ (SC-XRD) MAPLE = 88 843 kJ mol^{-1} Δ = 0.52%	K_2SO_4[27] + MoO_3[28] + SO_3[29] MAPLE = 88 382 kJ mol^{-1}
$Na_2[MoO_2(SO_4)_2]$ (SC-XRD) MAPLE = 88 660 kJ mol^{-1} Δ = 0.14%	Na_2O[30] + MoO_3[28] + 2 SO_3[29] MAPLE = 88 537 kJ mol^{-1}

occupation. Nevertheless, the calculated deviation stays below 1%.

UV-Vis and vibrational spectroscopy

The optical properties were investigated by UV-vis measurements. The recorded spectra reflect the colour of both products and consist of a ligand to metal charge transfer (LMCT) transition between oxygen and molybdenum ions in the UV region. The potassium compound β-$K_2[MoO_2(SO_4)_2]$ has a light blue colour due to a high reflection in the bluish region (Fig. 6). The samples seem to be stable under ambient conditions, as the UV-vis and the FT-IR spectra do not show large differences after several weeks of storage (Fig. S6). The sodium compound $Na_2[MoO_2(SO_4)_2]$ appears white to light green due to large reflections in the visible regime. The powdered samples are affected by moisture and show changes in colour with time which are observed in the UV-vis measurements as well (Fig. 7). The first change appears directly after opening the sample holder in air: the colour changes to a light blue. After 30 min, the blue becomes darker and then even darker after storing the sample overnight on the sample holder in air. This colour change comes with reaction with moisture, which is proven by the corresponding FT-IR spectra (Fig. S6). Here, the bands around 3400 cm^{-1} and 1600 cm^{-1} become pronounced. The band at 1600 cm^{-1} indicates the presence of free

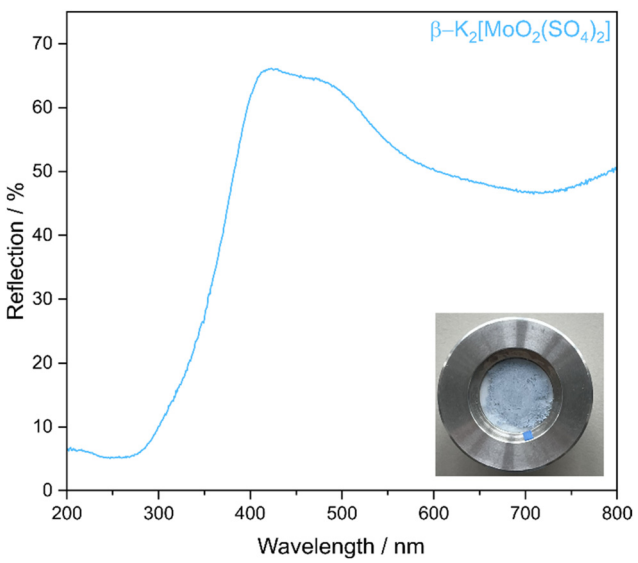

Fig. 6 UV-vis spectrum and picture of the colour impression of β-$K_2[MoO_2(SO_4)_2]$.

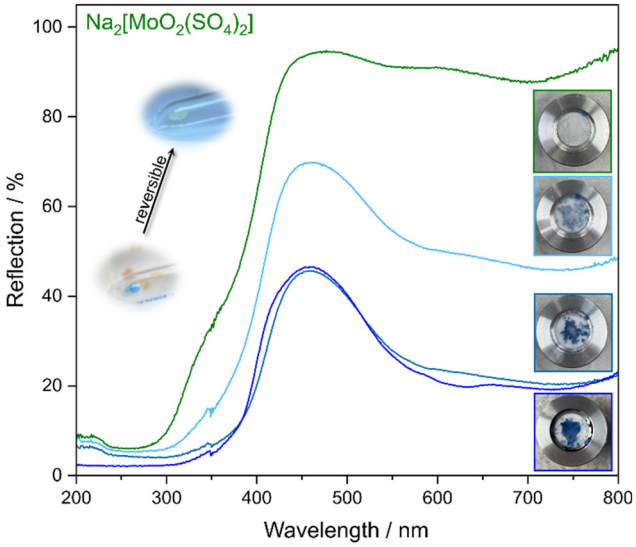

Fig. 7 UV-vis spectra and colour impressions of $Na_2[MoO_2(SO_4)_2]$ which change with time: dark green directly after opening the ampoule; light blue after exposing to air; medium blue after 30 min; and dark blue after one night.

H_2O molecules and no bonded hydroxyl groups.[31] The FT-IR spectra also indicate that $Na_2[MoO_2(SO_4)_2]$ starts to decompose in air after 30 min, since the bands between 1300 and 400 cm^{-1} start to broaden and differ. A similar blue colour change was observed in γ-$K_2[MoO_2(SO_4)_2]$,[12] although the phenomenon was not further discussed then. It is obvious that the colour originates from the d–d transitions of molybdenum in the visible regime. Recently, we proved the minimal presence of Mo^{5+} cations in the dark blue coloured α-$K_2[MoO_2(SO_4)_2]$, even though the sum formula would suggest only Mo^{6+} ions.[11] The different oxidation states of molybdenum enable its different colours, as also observed in molybdenum bronzes which are intensely blue samples due to the presence of Mo^{5+}. The contact of $Na_2[MoO_2(SO_4)_2]$ with ambient air and moisture most probably leads to a decomposition of the material and a simultaneous reduction of the molybdenum cations to Mo^{5+} and Mo^{4+}, both of which exhibit intensely blue coloured compounds.[32–35]

It is worth mentioning is that, in case of non-grinded samples, the colour switch of $Na_2[MoO_2(SO_4)_2]$ is reversible by heating again in a sealed ampoule at 280 °C. If only the surface is affected by moisture, the colour switch from blue to greenish $Na_2[MoO_2(SO_4)_2]$ is reversible. It becomes irreversible with grinded samples, since the water has penetrated the whole powder, apparently.

The vibrational bands in the FT-IR spectra for β-$K_2[MoO_2(SO_4)_2]$ and $Na_2[MoO_2(SO_4)_2]$ (Fig. 8) are very similar to α-$K_2[MoO_2(SO_4)_2]$[11] and can be assigned as described previously towards symmetric, antisymmetric and bending vibrations of Mo–O and S–O (Table S9). The absence of broad bands around 3400 and 1600 cm^{-1} proves the absence of hydroxyl groups or water in the materials.

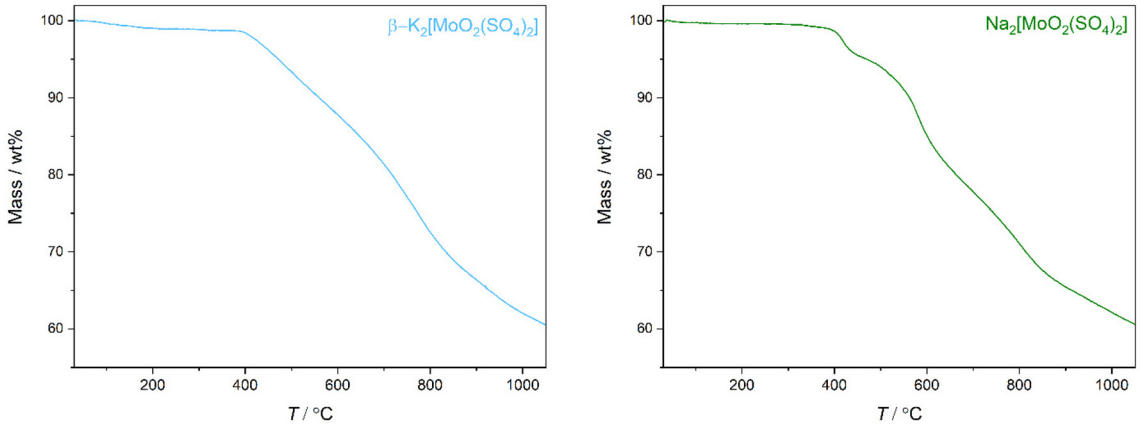

Fig. 8 FT-IR spectra of β-$K_2[MoO_2(SO_4)_2]$ and $Na_2[MoO_2(SO_4)_2]$. For the potassium compound, a comparison with the other polymorph α-$K_2[MoO_2(SO_4)_2]$ is shown.

We could not detect any luminescence in the titled compounds.

Thermal analysis

Both compounds, β-$K_2[MoO_2(SO_4)_2]$ and $Na_2[MoO_2(SO_4)_2]$, show-despite their highly charged sulfur and molybdenum centres-remarkably high thermal stabilities after investigations with thermogravimetric analysis in N_2 atmosphere (Fig. 9). β-$K_2[MoO_2(SO_4)_2]$ is stable up to 403 °C and $Na_2[MoO_2(SO_4)_2]$ until 420 °C. Both apparently decompose by releasing SO_3. The thermal stabilities of the titled compounds are comparable to those of the other sulfatomolybdates discovered so far (Table 4). A trend is apparent in this series; higher dimensionalities of the anion lead to lower thermal stabilities of the compound, also observed in borosulfate and sulfatotungstate chemistry.[11,36,37] A reason might be the large repulsion of the building units which becomes larger with higher densities in the materials.

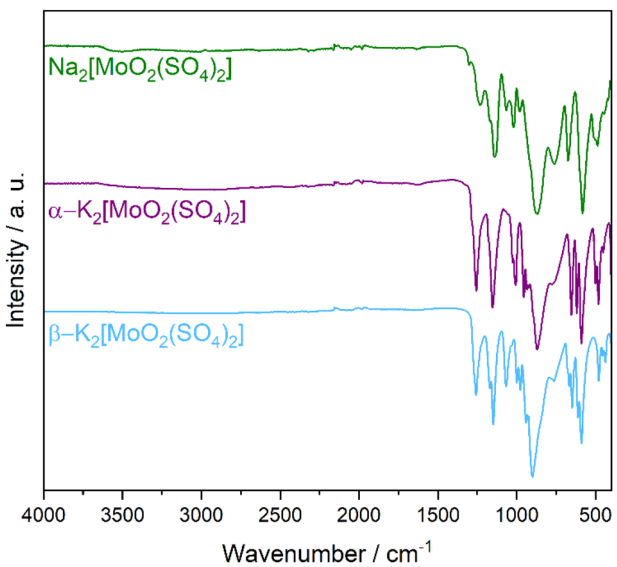

Fig. 9 Thermogravimetric analysis of β-$K_2[MoO_2(SO_4)_2]$ (left) and $Na_2[MoO_2(SO_4)_2]$ (right).

Table 4 Thermal stabilities of the titled compounds compared with those of other sulfatomolybdates and their respective anion dimensionalities

Compound	Thermal stability (°C)	Dimensionality
α-$K_2[MoO_2(SO_4)_2]$	390	3
β-$K_2[MoO_2(SO_4)_2]$	403	2
γ-$K_2[MoO_2(SO_4)_2]$	405	1
$K_8[(MoO_2)_2(SO_4)_6]$	560	0
$Na_2[MoO_2(SO_4)_2]$	420	2
$Na_4[MoO_2(SO_4)_3]$	436	1

Magnetic characterization

The temperature dependence of the magnetic susceptibility of $Na_2[MoO_2(SO_4)_2]$ and $K_2[MoO_2(SO_4)_2]$ (10 kOe data) is shown in Fig. 10. Both sulfatomolybdates show diamagnetic signals and two different types of upturns in the low-temperature regimes, starting at around 80 K for the $Na_2[MoO_2(SO_4)_2]$ and around 100 K for the $K_2[MoO_2(SO_4)_2]$ sample. These upturns most likely result from tiny amounts of paramagnetic impurities ('Curie tails'). In order to be able to classify the experimental values, we calculated the molar susceptibilities of both compounds from the diamagnetic increments (-1.42×10^{-4} emu mol^{-1} for $Na_2[MoO_2(SO_4)_2]$ and -1.588×10^{-4} emu mol^{-1} for $K_2[MoO_2(SO_4)_2]$), taking the values from Bain and Berry.[38] The experimental values almost fit the increment sums. After subtraction of the increment sums, still, very small diamagnetic values remain at room temperature. Thus, the magnetic data give no definite proof for small degrees of pentavalent molybdenum. Color changes in such oxides can already occur with tiny losses of oxygen. The remaining amount of reduced transition metals is too small to be detected. Such behavior was also observed for the yellow rhenates $Ca_5Re_2O_{12}$ and $Sr_5Re_2O_{12}$, which turn green when annealed at 1000 °C.[39]

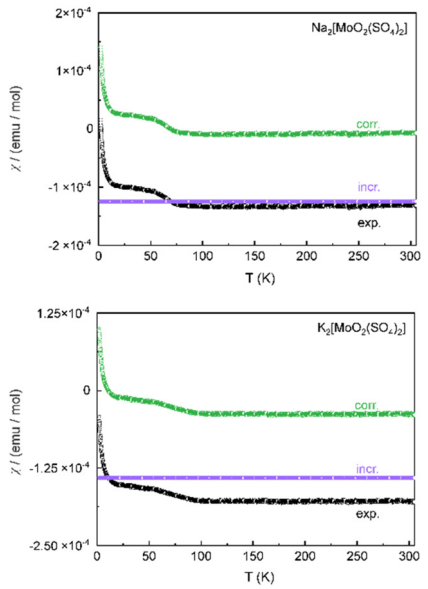

Fig. 10 Temperature dependence of the magnetic susceptibility of $Na_2[MoO_2(SO_4)_2]$ and $K_2[MoO_2(SO_4)_2]$. The experimental data are shown as black dots. Magenta and green dots correspond to the susceptibilities calculated from diamagnetic increments and the susceptibilities obtained after subtraction of the core diamagnetism, respectively.

Experimental section

Synthesis

$Na_2[MoO_2(SO_4)_2]$ and β-$K_2[MoO_2(SO_4)_2]$ were prepared *via* solid state synthesis and melting the reactants. Initially, $K_2S_2O_7$ (0.5 mmol, Bernd Kraft) or $Na_2S_2O_7$ (0.5 mmol) and MoO_3 (0.5 mmol, Fluka) were ground stoichiometrically. $Na_2S_2O_7$ was prepared *via* heating $NaHSO_4$ at 250 °C according to the reaction $2\ NaHSO_4 \rightarrow Na_2S_2O_7 + H_2O$. The reactants $K_2S_2O_7$ and $Na_2S_2O_7$ were stored in a drying cabinet at 180 °C before use. The ground reactants were loaded into a silica ampoule and torch sealed under vacuum (4×10^{-2} mbar). Two furnace steps are necessary. In the first one, the reactants were dissolved in $A_2S_2O_7$ (A = Na, K) at 430 °C, held for 10 h and cooled to room temperature over 80 h. Before furnace step two is applied, the reactants need to be ground again. In the case of $Na_2[MoO_2(SO_4)_2]$, the ambient conditions during the grinding process are not relevant, but they become important for β-$K_2[MoO_2(SO_4)_2]$, which has to be ground under argon conditions in an argon box. When ground under ambient air, the phase α-$K_2[MoO_2(SO_4)_2]$ forms. Eventually, the amorphous powders were transferred again to a silica ampoule and vacuum sealed before heating to 230 °C, holding for 2 h, cooling to 145 °C over 23 h and cooling to room temperature over 1 h. Phase pure powders and single crystals were obtained by the described technique, light green in the case of $Na_2[MoO_2(SO_4)_2]$ and light blue in the case of β-$K_2[MoO_2(SO_4)_2]$. $Na_2[MoO_2(SO_4)_2]$ can also be prepared without evacuated ampoules by just sealing the ampoules under air. Nevertheless, in both cases, the received product should be stored in an argon box. β-$K_2[MoO_2(SO_4)_2]$ seems to be stable in ambient conditions.

Crystal structure determination

Single crystals were transferred into perfluorinated polyether after opening the ampoules and selected for single-crystal X-ray diffraction measurements under a polarising microscope. Diffraction data were collected with a Bruker D8 Venture diffractometer using Mo-Kα radiation (λ = 0.71073 A). For high temperature measurements, the temperature was adjusted with a nitrogen flow using an Oxford cryo-system. The absorption correction was performed by employing the multi-scan method. The crystal structures of β-$K_2[MoO_2(SO_4)_2]$ and $Na_2[MoO_2(SO_4)_2]$ at high temperatures were solved by direct methods within the SHELXS program and refined by the full-matrix least-squares technique within the SHELXTL software package.[40,41] The crystal structure of $Na_2[MoO_2(SO_4)_2]$ at room temperature was solved and refined using Jana 2020.[26] During the refinement, modulated displacement functions were employed for all atoms and additional occupational ones for the sodium atoms. The occupation of the latter was refined freely. The *q*-vector was determined using the software package APEX6 from Bruker.[42] Relevant crystallographic data and further details of the structure determination are summarised in Table 2 and S1–S7.

X-ray powder diffraction

The samples were ground and placed in a Hilgenberg silica glass capillary with a wall thickness of 0.01 mm and an outer diameter of 0.3 mm. Data were collected with a Bruker D8 Advance diffractometer using Cu-K_α radiation (λ = 1.54184 A) with a 1D LynxEye detector system, steps of 0.02° and transmission geometry. The generator was operated at 40 kV and 40 mA. The high background at low diffraction angles appears due to the absorption of the glass capillary.

Infrared spectroscopy

The infrared spectra were recorded at room temperature using a Bruker EQUINOX 55 FTIR spectrometer equipped with a platinum ATR setup in the range 4000–400 cm^{-1}, a resolution of 2 cm^{-1} and 32 scans per sample.

Optical spectroscopy

The UV-vis spectra were measured as diffuse reflection spectra with a Varian Cary 200 Scan UV-vis spectrophotometer equipped with an Ulbricht sphere and deuterium and mercury lamps. The lamp switch occurs at 350 nm. The scan range was 200–800 nm with an increment of 1 nm and a scan rate of 120 nm cm^{-1}.

Thermal analysis

Thermogravimetric analysis (TGA) was done in alumina crucibles using a NETZSCH STA 409 PC Luxx in nitrogen atmosphere and a heating ramp of 5 K min^{-1}.

Magnetic susceptibility measurements

Powders of $Na_2[MoO_2(SO_4)_2]$ and $K_2[MoO_2(SO_4)_2]$ were weighed and placed into polypropylene capsules. The capsules were

attached to a brass sample holder and studied with the VSM (vibrating sample magnetometer) option of a Dynacool physical property measurement system (PPMS). Zero-field-cooling measurements were run in the temperature range 2–305 K with a flux density of 10 kOe.

Conclusions

Herein, we elucidated the two new sulfatomolybdates $Na_2[MoO_2(SO_4)_2]$ and β-$K_2[MoO_2(SO_4)_2]$, the first ones possessing 2D anionic substructures. $Na_2[MoO_2(SO_4)_2]$ exhibited an incommensurately modulated structure at room temperature with disorder and reduced occupation of the sodium cations, which meander through the anion layers. The modulation orders when raising the temperature to 100 °C, while the disorder remains. The structural models were confirmed by MAPLE calculations. The polymorph β-$K_2[MoO_2(SO_4)_2]$ (2D) makes the third of the described sum formula, next to α-$K_2[MoO_2(SO_4)_2]$ (3D) and γ-$K_2[MoO_2(SO_4)_2]$ (1D). All the polymorphs comprise different anion dimensions, decreasing with the amount of *vierer rings* built up by connected fundamental building units. To achieve the different polymorphs, the reaction conditions must be chosen carefully by selecting the right pressure and the environmental gases during the grinding process. The colours of the title compounds can be attributed to the d–d transitions of molybdenum. While β-$K_2[MoO_2(SO_4)_2]$ seems to be stable at ambient conditions, $Na_2[MoO_2(SO_4)_2]$ decomposes on contact with moisture, as noted in connection with a colour change detected by UV-vis spectroscopy. The intensities of the d–d transitions increase with moisture, leading to a dark blue colour. Remarkably, the colour change is reversible for non-ground samples. Despite their highly charged polyhedral centres, the title compounds show fairly high thermal stabilities above 400 °C, as determined by thermogravimetric analysis.

There is no doubt that these slightly coloured layered compounds, especially the sodium analogue, are highly interesting. Their reversible, deliberate reduction suggests that they could serve as viable electrode materials. This will be explored in future work soon.

Author contributions

Henning Höppe: design and supervision of the study and writing; Vivien Wessels: design and conduction of syntheses of the samples, general characterisation supervision of the measurements, and writing, Jasper Arne Baldauf and Rainer Pöttgen: magnetic characterisation.

Conflicts of interest

There are no conflicts of interest.

Data availability

Data for this article, such as the crystallographic data including CIF files, are available from the ICSD at https://www.ccdc.cam.ac.uk/structures/. The respective CSD numbers are listed in Table 2 of the manuscript. Further data supporting this article have been included as part of the supplementary information (SI). Details of the software employed for the investigations presented are given in the Experimental section.

Supplementary information is available. See DOI: https://doi.org/10.1039/d5dt03061g.

CSD 2518135–2518137 contain the supplementary crystallographic data for this paper.[43a–c]

Acknowledgements

This research was funded by Universität Münster and Deutsche Forschungsgemeinschaft (INST 211/1034-1 for R.P. and J.A.B. as well as project 556118528 for H.A.H. and V.W.).

References

1 C. Delmas, D. Carlier and M. Guignard, *Adv. Energy Mater.*, 2021, **11**, 1271–1279.
2 U.-H. Kim, D.-W. Jun, K.-J. Park, Q. Zhang, P. Kaghazchi, D. Aurbach, D. T. Major, G. Goobes, M. Dixit, N. Leifer, C. M. Wang, P. Yan, D. Ahn, K.-H. Kim, C. S. Yoon and Y.-K. Sun, *Energy Environ. Sci.*, 2018, **11**, 1271–1279.
3 H. Shang, F. Ning, B. Li, Y. Zuo, S. Lu and D. Xia, *ACS Appl. Mater. Interfaces*, 2018, **10**, 21349–21355.
4 J. Wu, J. Peng, H. Sun, Y. Guo, H. Liu, C. Wu and Y. Xie, *Adv. Mater.*, 2022, **34**, e2200425.
5 J. Bruns, H. A. Höppe, M. Daub, H. Hillebrecht and H. Huppertz, *Chem. – Eur. J.*, 2020, **26**, 7966–7980.
6 M. Daub, A. J. Lehner and H. A. Höppe, *Dalton Trans.*, 2012, **41**, 12121–12128.
7 H. A. Höppe and S. J. Sedlmaier, *Inorg. Chem.*, 2007, **46**, 3467–3474.
8 P. Netzsch, P. Gross, H. Takahashi and H. A. Höppe, *Inorg. Chem.*, 2018, **57**, 8530–8539.
9 P. Netzsch, M. Hämmer, P. Gross, H. Bariss, T. Block, L. Heletta, R. Pöttgen, J. Bruns, H. Huppertz and H. A. Höppe, *Dalton Trans.*, 2019, **48**, 4387–4397.
10 J. Fuchs, H.-U. Kreusler and A. Förster, *Z. Naturforsch.*, 1979, **34**, 1683–1685.
11 V. Wessels, F. Kraus, L. Bayarjargal, H.-A. Krug von Nidda, G. Eickerling and H. A. Höppe, *ChemistryEurope*, 2025, **3**, e202500275.
12 T. Noerbygaard, *Proc. Vol.*, 1998, **1998-11**, 553–573.
13 S. J. C. Schäffer and R. W. Berg, *Acta Crystallogr., Sect. E: Struct. Rep. Online*, 2008, **64**, i73.
14 S. J. C. Schäffer and R. W. Berg, *Acta Crystallogr., Sect. E: Struct. Rep. Online*, 2008, **64**, i20.

15 K. V. Dorn, B. Blaschkowski, P. Netzsch, H. A. Höppe and I. Hartenbach, *Inorg. Chem.*, 2019, **58**, 8308–8315.
16 P. Kaur, R. Kumar, S. Davessar and A. Khanna, *Acta Crystallogr., Sect. B: Struct. Sci., Cryst. Eng. Mater.*, 2020, **76**, 926–938.
17 T. Balić Žunić and E. Makovicky, *Acta Crystallogr., Sect. B: Struct. Sci.*, 1996, **52**, 78–81.
18 E. Makovicky and T. Balić-Žunić, *Acta Crystallogr., Sect. B: Struct. Sci.*, 1998, **54**, 766–773.
19 R. D. Shannon, *Acta Crystallogr., Sect. A*, 1976, **32**, 751–767.
20 R. Hübenthal, *MAPLE. Program for the Calculation of the Madelung Part of Lattice Energy*, University of Gießen, Germany, 1993.
21 R. Hoppe, *Z. Naturforsch.*, 1995, **50**, 555–567.
22 R. Hoppe, *Angew. Chem., Int. Ed. Engl.*, 1970, **9**, 25–34.
23 R. Hoppe, *Angew. Chem., Int. Ed. Engl.*, 1966, **5**, 95–106.
24 A. Arfaoui, B. Ouni, S. Touihri, A. Mhamdi, A. Labidi and T. Manoubi, *Opt. Mater.*, 2015, **45**, 109–120.
25 G. Leftheriotis, S. Papaefthimiou, P. Yianoulis and A. Siokou, *Thin Solid Films*, 2001, **384**, 298–306.
26 L. Palatinus, J. Plášil and M. Dušek, *Z. Kristallogr.*, 2023, **238**, 271–282.
27 N. V. Zubkova, I. V. Pekov, D. A. Ksenofontov, V. O. Yapaskurt, D. Y. Pushcharovsky and E. G. Sidorov, *Dokl. Earth Sci.*, 2018, **479**, 339–341.
28 L. Kihlborg, *Ark. Kemi*, 1963, **21**, 357–364.
29 R. Pascard and C. Pascard-Billy, *Acta Crystallogr.*, 1965, **18**, 830–834.
30 E. Zintl, A. Harder and B. Dauth, *Z. Elektrochem. Angew. Phys. Chem.*, 1934, **40**, 588–593.
31 K. Nakamoto, *Infrared and Raman Spectra of Inorganic and Coordination Compounds*, Wiley, 2008.
32 E. Riedel and C. Janiak, *Anorganische Chemie*, De Gruyter, Berlin, 8th edn, 2011.
33 A. Wold, W. Kunnmann, R. J. Arnott and A. Ferretti, *Inorg. Chem.*, 1964, **3**, 545–547.
34 M. Greenblatt, *Chem. Rev.*, 1988, **88**, 31–53.
35 J. Graham and A. D. Wadsley, *Acta Crystallogr.*, 1966, **20**, 93–100.
36 E. Turgunbajew and H. A. Höppe, *Angew. Chem., Int. Ed.*, 2025, e202424952.
37 V. Wessels, S. Kügle and H. A. Höppe, *Dalton Trans.*, 2024, **53**, 15703–15712.
38 G. A. Bain and J. F. Berry, *J. Chem. Educ.*, 2008, **85**, 532.
39 H. A. Mons, M. S. Schriewer and W. Jeitschko, *J. Solid State Chem.*, 1992, **99**, 149–157.
40 G. M. Sheldrick, *SHELXTL*, Bruker AXS, Karlsruhe, Germany, 2003.
41 G. M. Sheldrick, *Acta Crystallogr., Sect. C:Struct. Chem.*, 2015, **71**, 3–8.
42 *APEX VI*, Bruker AXS Inc., Madison, Wisconsin, USA, 2025.
43 (*a*) CSD 2518135: Experimental Crystal Structure Determination, 2026, DOI: 10.25505/fiz.icsd.cc2qjb5s.; (*b*) CSD 2518136: Experimental Crystal Structure Determination, 2026, DOI: 10.25505/fiz.icsd.cc2qjb6t; (*c*) CSD 2518137: Experimental Crystal Structure Determination, 2026, DOI: 10.25505/fiz.icsd.cc2qjb7v.